Journal of Transportation Technologies, 2026, 16(1), 115-132
https://www.scirp.org/journal/jtts
ISSN Online: 2160-0481
ISSN Print: 2160-0473

Evaluation of Air-Coupled Acoustic Emission Detection for Internal Rail Defects

Lei Jia[1], Jee Wong Park[1], Ming Zhu[2], Yingtao Jiang[2], Lihao Qiu[2], Hualiang Teng[1*]

[1]Department of Civil and Environmental Engineering and Construction, University of Nevada, Las Vegas, Las Vegas, NV, USA
[2]Department of Electrical and Computer Engineering, University of Nevada, Las Vegas, Las Vegas, NV, USA
Email: *hualiang.teng@unlv.edu

How to cite this paper: Jia, L., Park, J.W., Zhu, M., Jiang, Y.T., Qiu, L.H. and Teng, H.L. (2026) Evaluation of Air-Coupled Acoustic Emission Detection for Internal Rail Defects. *Journal of Transportation Technologies*, **16**, 115-132.
https://doi.org/10.4236/jtts.2026.161007

Received: October 6, 2025
Accepted: December 19, 2025
Published: December 22, 2025

Abstract

Internal rail defects present significant safety risks. Acoustic Emission (AE) technology has emerged as a promising technique for detecting these defects. The goal of this research is to investigate the characteristics of AE signals from internal rail defects by employing air-coupled optical microphones. This first phase of the research was to evaluate the propagation characteristics of AE signals in lab-controlled pencil lead break (PLB) tests with two scenarios: signal attenuation in the air and within the rail. These tests were particularly designed to assess the prototype's performance under varying conditions. The second phase involved real-world field tests at two test sites: the Nevada State Railroad Museum and the MxV Rail in Colorado. Data collected from both sites were analyzed to assess the effectiveness of detecting defects in rail. The test results revealed two key findings. First, the AE detection rate varied significantly between tests: 8.3% in the Nevada field test and 13.3% in the MxV Rail test. This difference suggests that AE detection rates may be influenced by defect size and conditions in the field environment. Second, wavelet packet power (WPP) analysis highlighted clear differences between PLB-induced AE signals and those from actual rail defects. While PLB signals displayed broader energy distribution across the frequency range, the AE signals from rail defects exhibited concentrated and intense peaks within the 100 - 160 kHz range. Overall, the non-contact sensor system demonstrated promise for detecting internal rail defects, effectively capturing AE signals.

Keywords

Railroad Infrastructure, Rail Defect Detection, Rail Health Monitoring, Wavelet Analysis, Acoustic Emission Detection

1. Introduction

Internal defects in rail are invisible from view, making traditional visual inspections ineffective. In response to this challenge, ultrasonic inspection techniques have been established to detect these defects. In these inspection techniques, ultrasonic waves reflect off internal defects and return to an employed ultrasonic sensor for analysis. Guided-wave defect detection in rails has also been applied for non-contact testing [1]. Laser ultrasonics was proposed as another non-contact detection technique. Acoustic Emission (AE) technology detects elastic waves generated by internal structural changes in the rail that could be caused by a sudden change in internal stress or an external impact, for example, from wheel and rail interaction. It generally has a frequency range from 20 kHz to 1 MHz. The research [2] indicates that the AE wave generated in the rails can be detected by sensors attached to the rail. However, the study's applications in the real world are not practical because monitoring long-distance rail tracks would require an extensive network of sensors to cover the entire length.

Recently, it was found that air-coupled acoustic waves can detect both internal and external defects in rail [3]. The characteristics of the air-coupled AE wave enable the development of a non-contact sensor for detecting rail defects. In the air-coupled sensor, a monochromatic laser beam propagating through the medium in the presence of a sound field undergoes a small modulation of its optical wavelength, proportional to the local density and, therefore, sound pressure. The core element of the optical microphone used to detect this wavelength modulation is a miniaturized, rigid Fabry-Perot cavity consisting of two semi-reflective mirrors. The intensity of laser light reflected from such a cavity is given by the product of the input intensity and a transfer function. The round-trip phase shift depends on the laser wavelength and the mirror distance. Therefore, any change in the laser wavelength induced by the sound field causes a change in the light intensity reflected by the cavity which can be detected by a photodiode.

This research studies AE characteristics generated from internal defects in rail using an air-coupled sensor. The research includes 1) experimental studies for conducting lab tests, small-scale actual rail-train tests, as well as full scale real-world rail-train tests and 2) analytical studies using various algorithmic investigations to analyze AE signals in relation to defects. The research was divided into two stages, each with a distinct objective. The first objective was to investigate the feasibility, performance, and limitations of an air-coupled sensor for detecting AE signals in a controlled environment. This stage involved lab-controlled PLB tests, focusing on analyzing the characteristics of PLB-induced AE signals for defect identification and evaluating the performance of various AE identification algorithms. The second objective was to explore the AE signal characteristics and the detection performance of the air-coupled sensor in real-world field tests. The tests involved internal defects only, with follow-up analysis and evaluations focusing on the characteristics of the AE signals induced by both defect types. The conclusion of this objective provided insights into the effectiveness and current limita-

tions of the proposed approach for railroad health inspection in real-world applications.

2. Literature Review

Non-Contact Ultrasonic (NCU) utilizes ultrasonic waves without requiring physical contact between the sensor and the material being inspected. This NCU technology is widely used in structure health inspections. Past research [4] employed pulse-echo for rail scanning with excitation frequencies around 200 kHz, demonstrating its potential for detecting both artificial and real defects. Despite these findings, a major limitation was the very low speeds in static conditions, a common drawback of ultrasonic detection methods for effective real-world applications.

Guided-wave defect detection in rails has also been applied for non-contact testing. A research [1] developed a prototype system that showed the dominance of high frequency waves around 200 kHz. The penetration depth is related to the wavelength; hence, defect sizing is possible by monitoring different frequency bands of the propagating waves. The researchers at the University of California at San Diego [5] developed a novel non-contact ultrasonic rail inspection system, using a focused air-coupled transmitter, symmetrically placed air-coupled receivers, and a statistical algorithm to maximize true outliers (defects) and minimize false positives. Their results demonstrate excellent performance at low speeds between 1 and 5 mph and show promise at speeds of 10 and 15 mph.

Laser ultrasonics is another non-contact detection technique. The laser ultrasonic system employed an Nd: YAG pulse laser for ultrasonic wave generation and a laser Doppler vibrometer for signal measurement [6]. This method underscores the interaction of ultrasonic waves with defects, enabling the detection of both surface and subsurface anomalies at high speeds.

A passive extraction method has been used to isolate defect signals based on non-contact ultrasonic monitoring [7]. A defect inspection prototype using two arrays of air-coupled receivers was tested to collect ultrasonic waves. Normalized cross-correlation and deconvolution operations were used to isolate defect properties. Thier results noted rail lubrication is an uncertain factor that may affect the wheel-rail contact behavior, and further development is necessary to improve detection accuracy and more effective data processing.

AE waves are elastic signals generated by changes in the material's internal structure, which are typically caused by a sudden change in internal stress or external impact [8] [9]. These changes can include crack growth in the body, sectional displacement in material, phase change, fiber breakage, and decomposition. An AE testing system used to detect such changes primarily employs bone-conduction sensors.

Initial research with AE applications to rail defect inspection [8] showed potential in simple experimental tests. While it opened the doors for future research, it was yet limited. Later studies expanded this approach. AE detection of rail defects at high speed based on a rail-wheel test rig was performed in a study [10], proving

that their method could effectively detect rail defects over 77 mph. A multi-branch convolutional neural network (CNN) was employed to classify rail defects [11]. However, all of these systems relied on contact-based bone-conduction sensors, which are impractical for large-scale or real-time rail inspection due to their installation requirements of direct contact.

3. Testing Prototype

The testing prototype is shown in Figure 1. The prototype developed included data acquisition equipment, optical microphone sensors, pre-amplifiers, and high-speed cameras. Membrane-free Optical Microphone model Eta 250 was used in this study. The frequency range is 10 Hz - 1 MHz, dynamic range is 100 dB; and self-noise is 50 μPa. National Instrumental cRio 9041 with module NI 9223 were utilized as data acquisition (DAQ) equipment, the sampling rate was 1 MHz. Mistras 2/4/6 voltage preamplifiers (PAC 2/4/6) were employed to amplify the AE signals before they were recorded by DAQ equipment. The gain was set to 60 dB for all the tests to ensure the AE signal qualities. During the test, the band-pass filter was selected to be 20 - 500 kHz to eliminate the effects of low-frequency noises unrelated to the AE events. Labview was used to control data collection and storage. To ensure long-time data recording without interruption, the producer and consumer modules were employed to save current data and keep recording new data simultaneously. A go-pro camera was utilized to record geo-information during the field tests. It provides up to 240 frames video recording. Hammer hit was employed when each test started, to synchronize the time between video and AE signals.

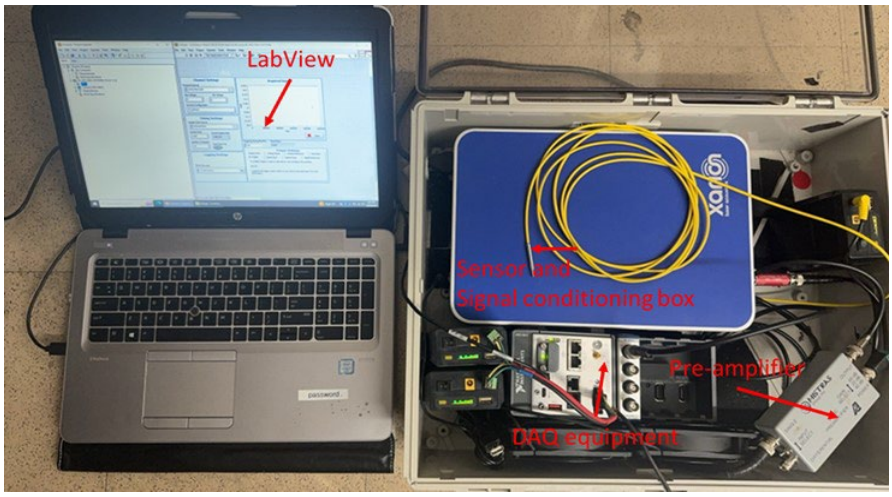

Figure 1. DAQ system schematic.

4. Investigation of Air-Coupled Sensor Performance in PLB Tests

This section addresses the first objective of the study: evaluating the feasibility, performance, and limitations of the air-coupled sensor in a controlled lab envi-

ronment. Pencil Lead Break tests were conducted to simulate AE events, allowing for detailed analysis of AE signal characteristics and sensor response under ideal conditions.

4.1. Pencil Lead Break Tests

The PLB test is commonly employed to replicate AE signals by breaking the tip of a pencil lead against the material surface. In this test, two distinct test scenarios were designed. The first test scenario as shown in **Figure 2(a)** focused on evaluating the attenuation of AE signals as they propagate through the rail. In this setup, the optical microphone was positioned near the rail surface to capture AE signals generated by PLB events. The pencil tip was carefully positioned at the cross-section of the rail head. The sensor was then moved longitudinally along the rail surface at varying distances from the PLB point, ranging from 0 to 3 inches in 0.5-inch increments.

The second test, as shown in **Figure 2(b)**, presents the test conducted to assess the attenuation characteristics of AE signals as they propagate through the air. In this setting, the sensor head was positioned at the side of the rail head, and the AE signals were evaluated at different distances from the source. The sensor head was installed at various distances above the rail surface, ranging from 0 to 3 inches in 0.5-inch increments.

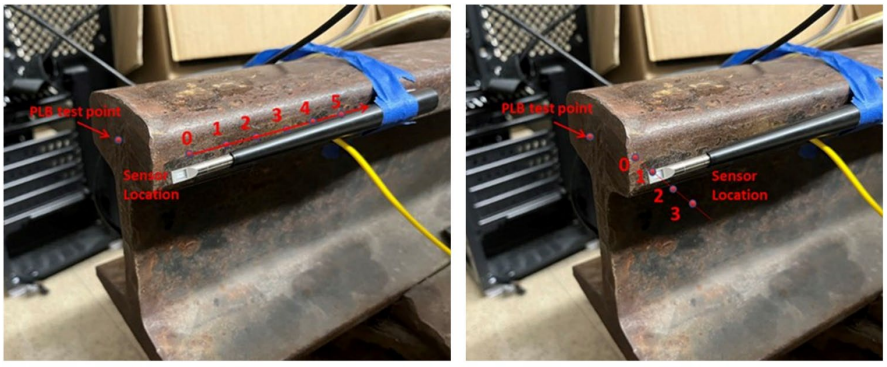

(a) (b)

Figure 2. Attenuation test for AE propagation (a) in the rail (b) in the air.

4.2. PLB Results and Discussion

The PLB test results and discussion focuses on time-frequency characteristics, signal attenuation behavior, and the effectiveness of wavelet-based AE signal identification. These findings establish a baseline for evaluating sensor performance in controlled conditions.

4.2.1. Time-Frequency Representation of AE Waves

The time-frequency characteristics of AE signals generated by PLB tests and real-world field tests were analyzed using Continuous Wavelet Transform (CWT). The analysis shows that the wave energy is predominantly concentrated in the low-frequency range of 20 - 40 kHz, with a notable portion also present in the high-

frequency range of 80 - 130 kHz. To enhance the identification of high-frequency features specific to PLB signals, a 100 kHz high-pass filter was applied. It is shown that the energy is primarily concentrated in the 120 - 170 kHz range for PLB signals.

4.2.2. Propagation Characteristics of AE Waves

Figure 3 presents amplitude attenuation results for PLB signals propagating through the rail. Using the plots in Figure 3, the amplitude attenuation of PLB signals in the rail is analyzed. The blue bars represent the amplitudes of the PLB signals filtered with the original 20 kHz high-pass filter, while the green bars show the signals filtered with a 100 kHz high-pass filter. The black I-shaped markers denote the maximum and minimum amplitude ranges for each distance.

- 20 kHz filter: Amplitude declined from 4.17 V to 1.46 V, with notable drop-off starting around 2.5 inches.

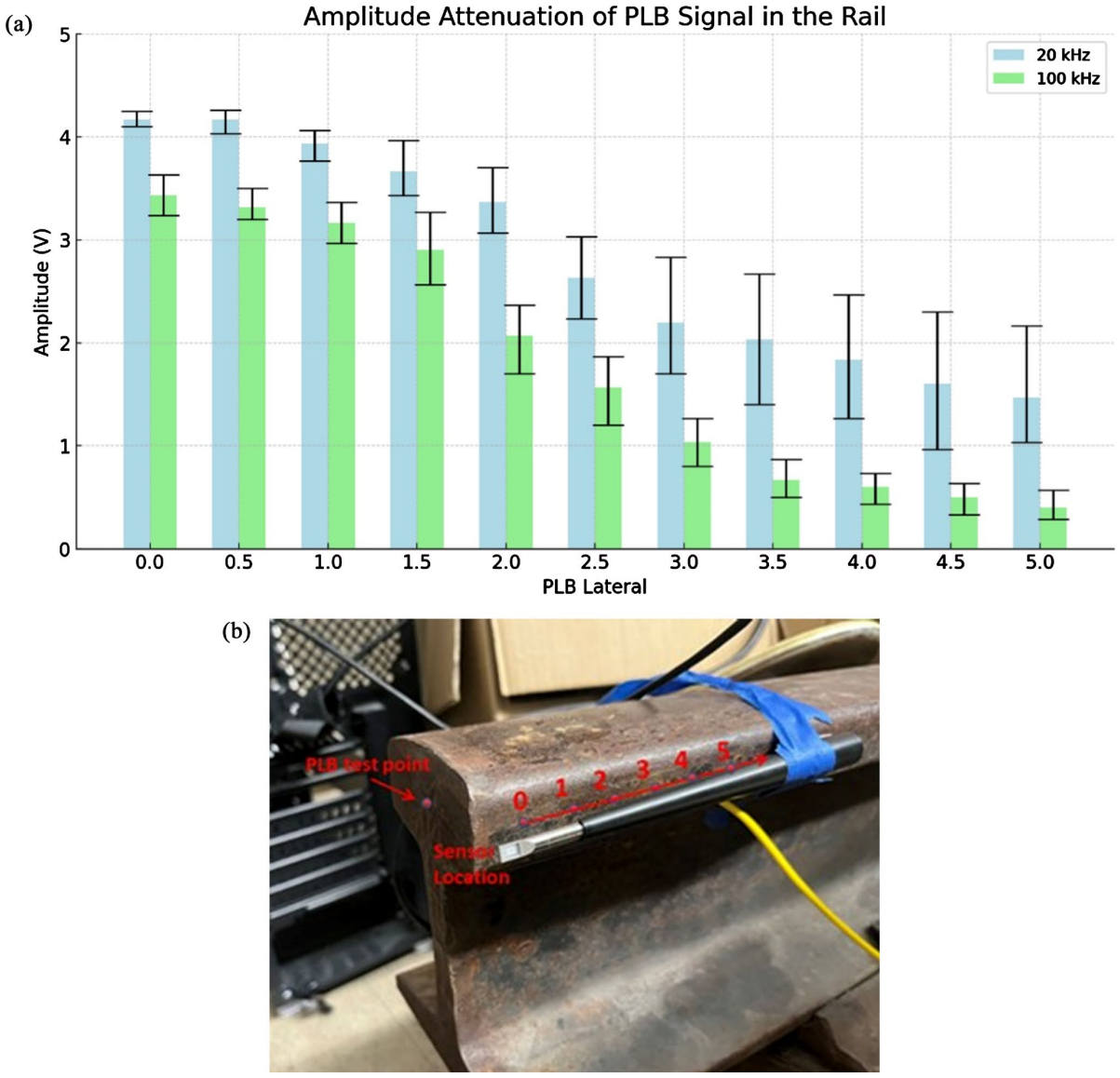

Figure 3. (a) Amplitude attenuation of PLB signal in the rail; (b) Test setup.

- 100 kHz filter: Amplitude declined from 3.43 V to 0.41 V, with sharper attenuation starting at 2 inches.

These results confirm that higher-frequency energy attenuates more rapidly than lower-frequency energy. Furthermore, the signals show greater relative fluctuation in amplitude beyond the 2-inch propagation distance. This variability indicates that PLB signals had difficulty maintaining a stable attenuation over long distances.

The attenuation characteristics in the air are shown in Figure 4. The data shows that the amplitude of the 20 kHz filter decreases from 4.25 V to 2.88 V, whereas the amplitude of the 100 kHz filter drops more dramatically from 3.43 V to 0.87 V as the distance increases from 0 to 3 inches. This indicates that the higher frequency components (100 kHz) experience more rapid attenuation than the

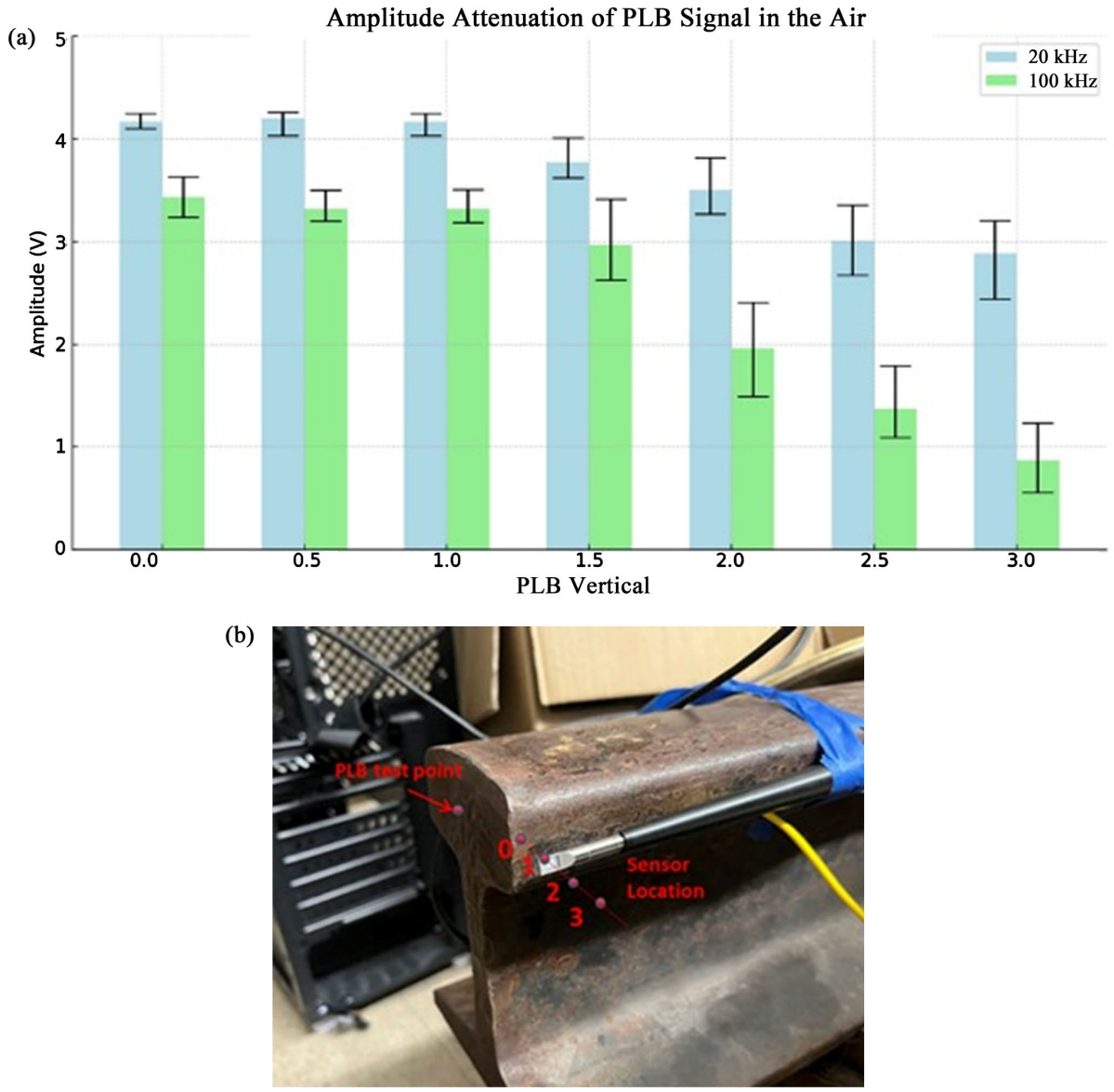

Figure 4. (a) Amplitude attenuation of PLB signal in the air; (b) Test setup.

lower frequency components (20 kHz). For the 20 kHz filter, a marked decline in amplitude is noted starting around 2.5 inches, suggesting that this filter retains more of the lower frequency energy over shorter distances before attenuating more noticeably. In contrast, the 100 kHz filter shows a rapid decrease in amplitude beginning at 2 inches, highlighting how the higher frequency signals are more susceptible to attenuation in the air. Additionally, both filters have more significant relative amplitude fluctuation beyond the 2-inch distance.

The findings suggest that to effectively capture high-frequency AE signals, the propagation distance within the rail should stay within 2 inches, and the sensor's proximity to the rail surface should also be maintained within 2 inches. Furthermore, the significant attenuation observed with the 100 kHz filter reduces the possibility of mistakenly identifying AE signals from defects located further away on the far side of the rail, which are induced by other wheel-rail impacts. It also enhances the accuracy of defect identification by ensuring that only signals from sensor-located wheel-rail impacts can be well captured, thereby reducing the likelihood of misidentification.

4.2.3. Wavelet Packet Power-Based AE Identification

In this study, the Wavelet Packet Transform (WPT)-based power analysis was utilized to exploit its advantage of uniform frequency resolution across all scales. To maintain consistency and ensure data quality in representing the AE characteristics, all Wavelet Packet Power (WPP) calculations were performed using the signals collected at 0-inch position across all scenarios. A high-pass filter with a cut-off frequency of 100 kHz was applied to the data to remove low-frequency noise.

The WPP spectrum and maxima present the typical energy distribution of signals collected from PLB tests. The power spectrums indicate that the energy is primarily concentrated within the 100 kHz to 300 kHz frequency range, with three distinct energy peaks around 100 - 140 kHz, 200 kHz, and 270 kHz. These peaks are consistent across multiple plots, suggesting repeatable features likely related to the AE characteristics of the PLB signal under the tested lab conditions.

5. Rail Internal Defect Detection Using Air-Coupled Sensors

This section focuses on the second objective of the study: assessing the real-world performance of the air-coupled sensor in detecting AE signals from internal rail defects. Field tests were conducted at two locations to evaluate the sensor's ability to detect and characterize AE signals under practical operating conditions.

5.1. Rail Internal Defect Detection in Nevada

This study evaluated rail internal defect detection by testing the air-coupled AE technique in two settings: rail-mounted field tests and vehicle-mounted field tests. The rail-mounted field test was conducted on a pre-damaged track at the Nevada State Railroad Museum. Two internal welding defects were used for evaluation. The dimensions and locations were identified using the Olympus Epoch 1000i ul-

trasonic inspector, as detailed in Figure 5. The sensor head was mounted onto a fixture attached to the rail surface by placing it below the rail head.

Welding defect: 0.3 in by 0.3 in. Location: 1.9 inches below the surface

Welding defect: 0.2 in by 0.3 in. Location: 2.5 inches below the surface

Figure 5. Internal defect location and size.

Similar to the PLB test setup, this rail-mounted field test examined AE attenuation in both rail and air, separately. Two configurations were evaluated as shown in Figure 6:

- Vertical sensor displacement: The sensor was moved vertically away from the railhead, as shown in Figure 6(a). Each subsequent test moved the sensor by one inch in the air.
- Horizontal sensor displacement: The sensor was moved laterally along the rail web as shown in Figure 6(b). Each subsequent test moved the sensor by two inches.

For these tests, an unloaded hopper car with an approximate axle load of 70,000 lb was employed. This car was capable of moving at speeds up to 5 mph.

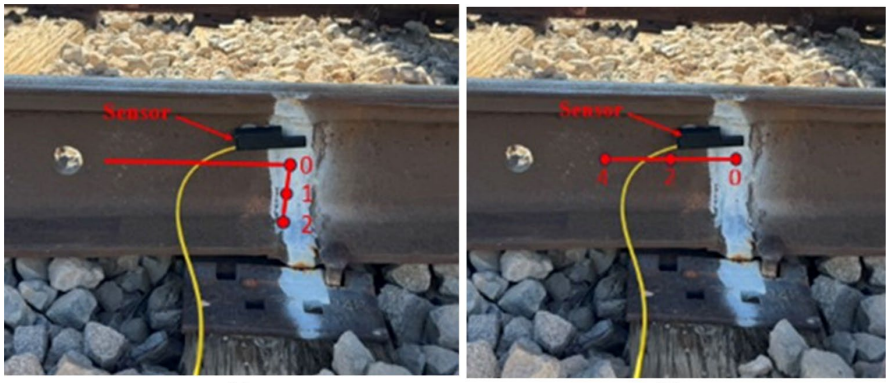

(a) (b)

Figure 6. Attenuation evaluation (a) vertically in the air; (b) longitudinally in the rail.

Vehicle-Mounted Field Tests

The vehicle-mounted test was conducted in the same configuration and procedures as in the rail-mounted tests, except for the sensor installation location. In this test, the sensor was installed on the mounting frame of the train, as shown in Figure 7. To ensure sensor safety (e.g., not colliding with the rail during the test operation), the sensor was placed 1.5 inches away from the rail head side.

As in the rail-mounted test, sensor positioning was systematically adjusted. Starting from the initial position (Figure 8), the sensor was laterally shifted 2 inches toward the far side of the rail for each subsequent test. This adjustment allowed evaluation of AE signal detection performance at varying horizontal offsets under realistic, vehicle-mounted conditions.

Figure 7. Mounting frame (front and side views).

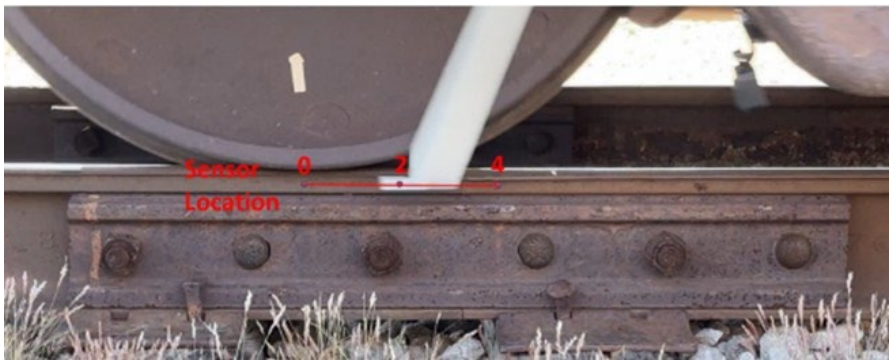

Figure 8. Attenuation evaluation in the rail (longitudinally).

5.2. Rail Internal Defect Detection at MxVRail in Colorado

During the initial tests conducted in Nevada, several challenges arose due to the site setup. Specifically, the existing joint bar configuration in the rail unexpectedly created significant joint bar impact noise, which obscured the detection of AE events. To address this limitation, additional field tests were conducted at MxV Rail in Colorado.

The Facility for Accelerated Service Testing (FAST) loop at MxV Rail was selected for its ability to naturally induce rail defects through the repeated loading of commercial hopper cars. This environment offered a more controlled and representative setting for evaluating AE detection under realistic service conditions.

As with the previous tests, the MxV Rail study included two test scenarios:

1) Rail-mounted configuration;

2) Vehicle-mounted configuration.

These tests aimed to validate the air-coupled AE technique under improved track conditions and to further assess its reliability for detecting internal rail defects in operational environments.

5.2.1. Rail-Mounted Field Test

The rail-mounted field test used two naturally generated internal defects shown in Figure 9. The larger defect measured 0.8 inches by 0.6 inches and was situated 0.7 inches below the top surface, indicating that it was in the late stage of development. In contrast, the smaller defect, measuring 0.3 inches by 0.3 inches and located 0.6 inches below the top surface, was still in the early stage of development.

Welding defect 1: 0.8 in x 0.6 in. Location: 0.7 inches below the surface

Welding defect 2: 0.3 in x 0.3 in. Location: 0.6 inches below the surface

Figure 9. The internal defects.

In this test, the sensor head was mounted onto the rail surface. The sensor was placed under the rail head at the defect location, at distances of 0, 1, and 2 inches from the defect. In the air, the sensor was placed at the same location but then moved laterally to the left by 0, 2, and 4 inches. Six unloaded hopper cars, each with an approximate axle load of 70,000 pounds, and a locomotive weighing approximately 432,000 pounds were used. Each test included 10 repeat runs, with the testing speed set to 5 mph. The tests resulted in 28 rail-wheel impacts per back-and-forth test run, each capable of generating AE events.

5.2.2. Vehicle-Mounted Field Test

In this testing scenario, the sensor was installed the same way as in the Nevada tests. It was mounted on the train's frame, and acoustic signals were recorded when the train passed over the defects. The sensor was positioned safely 1.5 inches away from the side of the rail head. As in previous tests, the sensor was relocated from its original position to the far side of the defect by moving it from 0 to 4 inches at two inches increment.

6. Results and Discussion

This section presents the key findings from both laboratory and field tests, high-

lighting the detection performance, signal characteristics, and analysis results of AE signals captured using the air-coupled sensor system. Each subsection addresses a specific aspect of the results to evaluate the sensor's effectiveness in identifying internal rail defects under varying conditions.

6.1. AE Events Detection Rate

To better present the performance of AE event detection, this section summarizes the total AE events observed during the field tests. Due to the inherent variability and uncertainty associated with on-vehicle testing conditions, AE events from these scenarios are not included in this section.

In the Nevada field test, two rail cars were utilized, resulting in 18 wheel-rail contact points per run, equating to a total of 540 hits based on the test configuration. From these, 45 significant AE events were detected, representing 8.3% of the total hits.

In contrast, the MxV Rail field test utilized six rail cars, producing 54 wheel-rail contacts per run and a total of 1740 hits. During these tests, 231 AE events were observed, accounting for 13.3% of the total hits.

The higher AE detection rate observed in the MxV Rail test may be attributed to the presence of larger defects compared to those in the Nevada test, indicating that the AE detection rate could be influenced by defect conditions. However, further investigation is required to validate this hypothesis and determine whether AE event detection can reliably serve as an indicator of rail defect progression.

6.2. Time-Frequency Representation of AE Waves

The time-frequency characteristics of AE signals generated during the real-world field tests were analyzed using CWT. The analysis presents that the wave energy is predominantly concentrated in the low-frequency range of 20 - 40 kHz, with a notable portion also present in the high-frequency range of 80 - 130 kHz. With a 100 kHz high-pass filter applied, the energy is primarily concentrated in the 110 - 140 kHz.

Moreover, distinctive pulse sequences were observed at two-time scales, where the signal attenuation is gradual, and each pulse exhibits a pattern of central energy concentration. These burst patterns across the two-time scales can also be observed. It is important to note that these repetitive patterns were not observed across all AE sources; they were not observed in PLB signals and were significantly less frequent in AE signals from the small rail defect than the large defect observed in MxV Rail tests.

Further investigation is required to fully understand the mechanisms behind these repetitive patterns and their correlation with defect size and the energy release process during defect growth. One hypothesis suggests that the first observed pattern (pattern 1) may result from multiple energy releases associated with incremental crack growth. However, it is more likely that these patterns are related to AE signals within the rail structure. No specific boundaries or discontinuities

have been identified that would align with the calculated distances based on the sound velocity in steel rails and the observed time intervals (approximately 2×10^{-4} seconds).

The second pattern (pattern 2) may be attributed to internal reflections within the rail head, leading to constructive interference and superposition of reflected waves. These initial hypotheses provide a basis for future research to clarify the relationship between these repetitive patterns and the physical characteristics of defects, including their size and progression in rail systems.

6.3. Propagation Characteristics of AE Waves

The amplitude attenuation of AE signals in both the rail and air indicates the challenges of capturing only relevant AE signal data in real-world scenarios, especially when compared to controlled laboratory PLB tests (Figure 10 and Figure 11). In PLB tests, signal amplitude typically attenuates clearly as the distance increases, which reflects a predictable decrease in energy due to propagation losses. However, in real-world field tests, this attenuation pattern is not as evident. In the attenuation plot of the rail scenario, AE signal amplitudes remain relatively stable or even slightly increasing without showing obvious AE signal attenuation of the AE signals. This unexpected behavior was likely due to the complicated and noisy environment of the field conditions, where numerous factors, such as strong wheel-rail impact noise, contribute to signal variability.

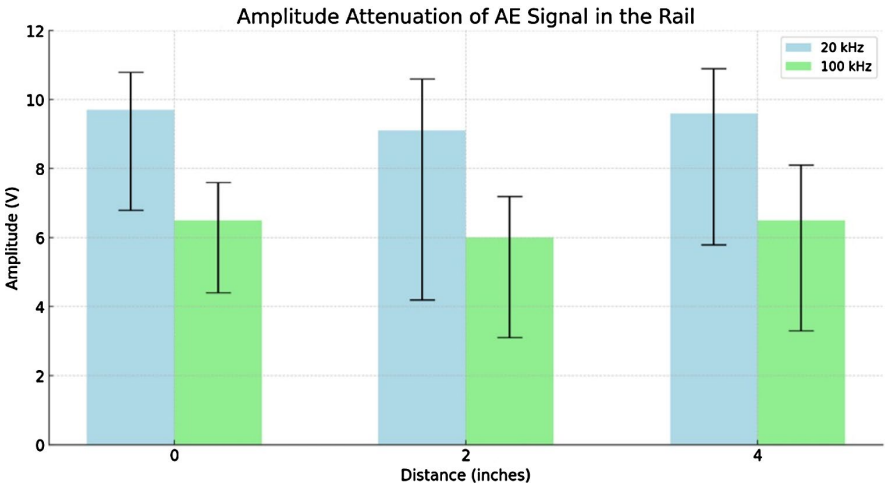

Figure 10. Amplitude attenuation of AE signal in the rail.

In the attenuation plot in the air scenario (Figure 11), an abnormal phenomenon is observed where the amplitude of the AE signals increases as the distance from the source increases. This unusual result is likely due to the increased gap between the sensor and the rail surface, which allows the sensor to pick up more mechanical vibrations from the train itself rather than just the intended AE signals. These vibrations, being of high energy and broader in frequency, can lead to unexpected increases in measured amplitude. In some cases, this even caused an

overflow in the data collected.

The data from both scenarios exhibit significant randomness and fail to present the consistent decreasing pattern of signal attenuation observed in PLB tests. This indicates the impact of ambient noise and mechanical vibrations on the measurements, due to the complexity of real-world field tests. To address these issues in future field tests, it is necessary to properly evaluate the ambient noise level to properly configure the pre-amplifiers and ensure appropriate sensor mounting to reduce the collection of unrelated ambient noise. This will help reduce the effects of overflow and reduce interference from ambient noise and mechanical vibrations.

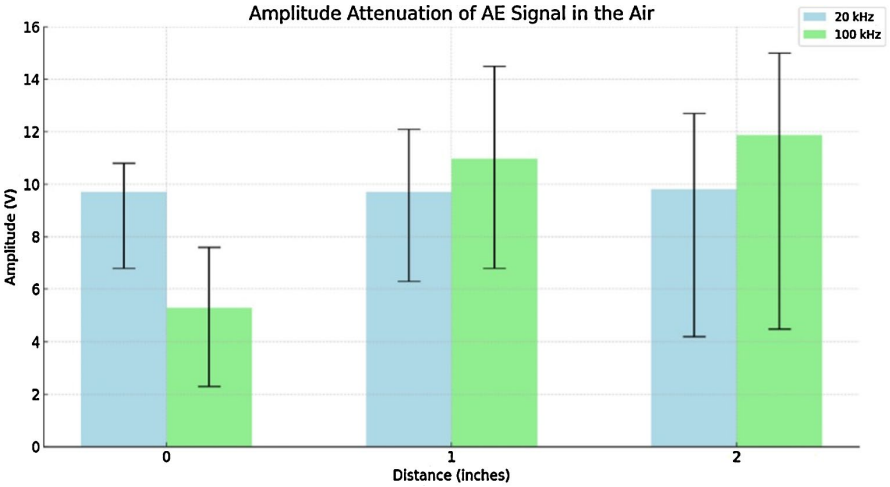

Figure 11. Amplitude attenuation of AE signal in the air.

6.4. Wavelet Packet Power-Based AE Identification

In this study, WPT-based power analysis is utilized to exploit the advantage of uniform frequency resolution across all scales. To ensure the data quality in presenting the AE characteristics, all the WPP calculations were performed using the signals collected at 0 inch from on-rail scenarios. A high-pass filter with a cutoff frequency of 100 kHz was applied to the data to better evaluate the AE characteristics in high-frequency range. As shown in Figure 12, the WPP spectrum and maxima present the typical energy distribution of signals collected from field tests. The rail defect AE signals predominantly display energy peaks within the 100 kHz to 160 kHz ranges. Unlike the broader energy distribution in the PLB signals, the rail defect spectra show highly concentrated peaks, reflecting stronger signal components likely associated with the severity of structural defects in the rail. Particularly, the rail defect signals demonstrate significantly higher power levels in the maxima plots, with peaks reaching up to 400, indicating more intense acoustic emissions compared to the PLB tests.

The rail defect AE signals are characterized by more evident and localized peaks, suggesting more severe energy releases. This difference features the importance of detailed frequency analysis in the 50 - 150 kHz range for distinguishing between AE sources. The increased power levels and distinct peak patterns in

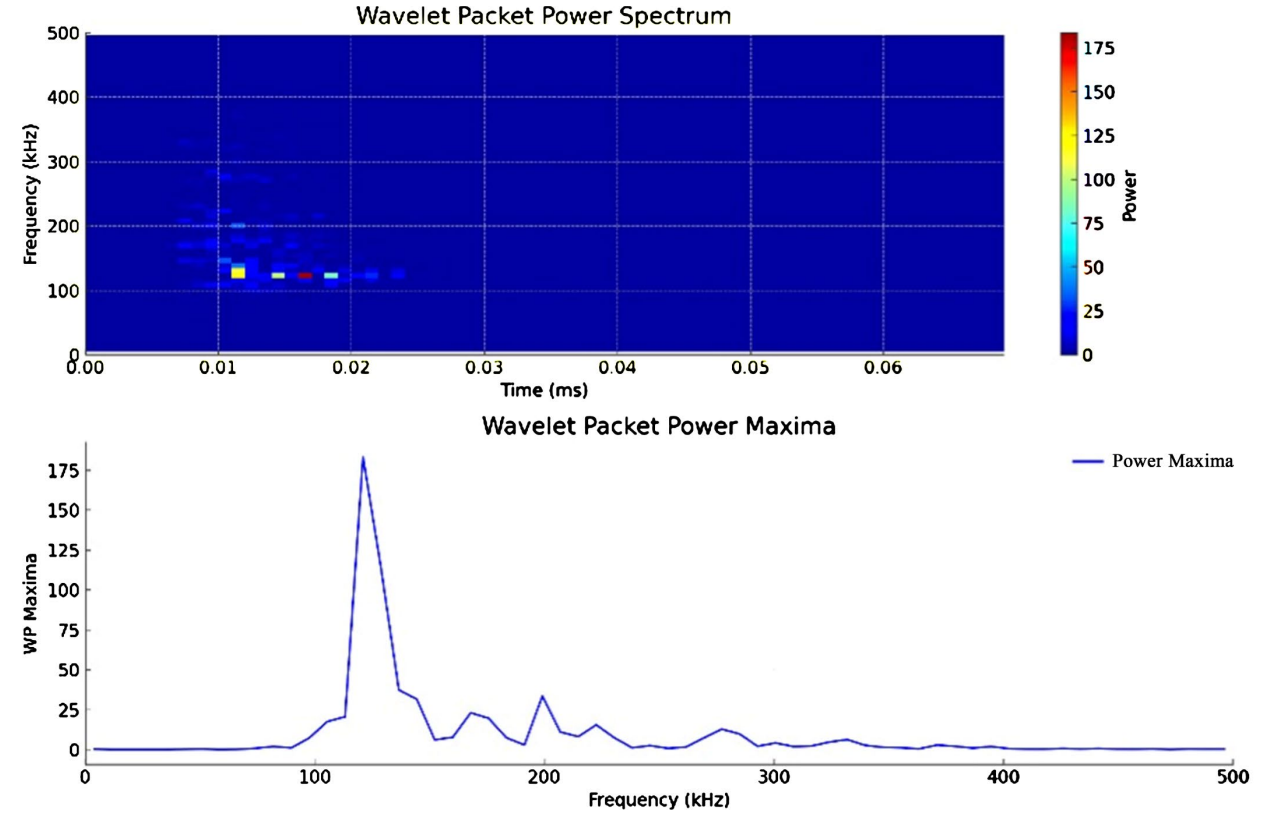
Wavelet Packet Power Spectrum
Frequency (kHz)
Time (ms)
Power
Wavelet Packet Power Maxima
WP Maxima
Frequency (kHz)
Power Maxima

(a)

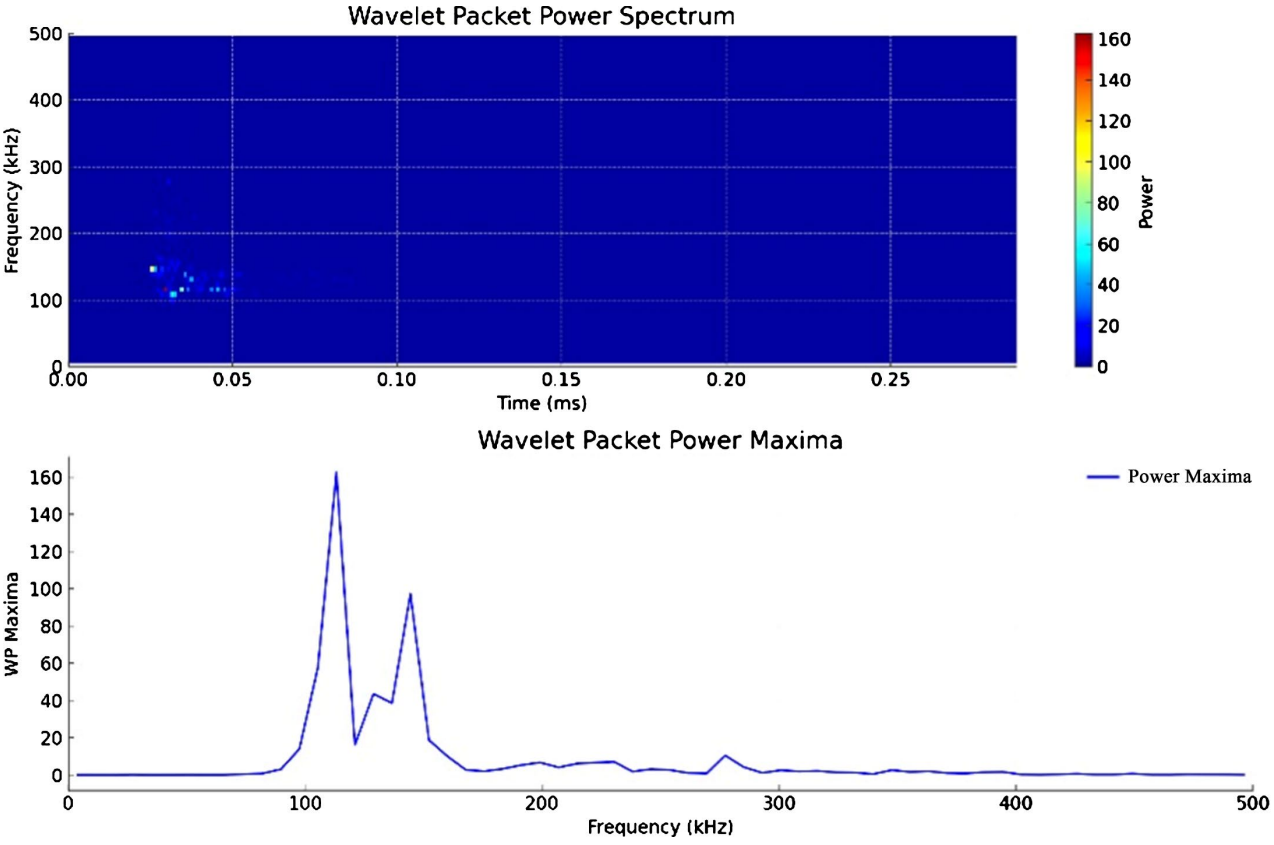
Wavelet Packet Power Spectrum
Frequency (kHz)
Time (ms)
Power
Wavelet Packet Power Maxima
WP Maxima
Frequency (kHz)
Power Maxima

(b)

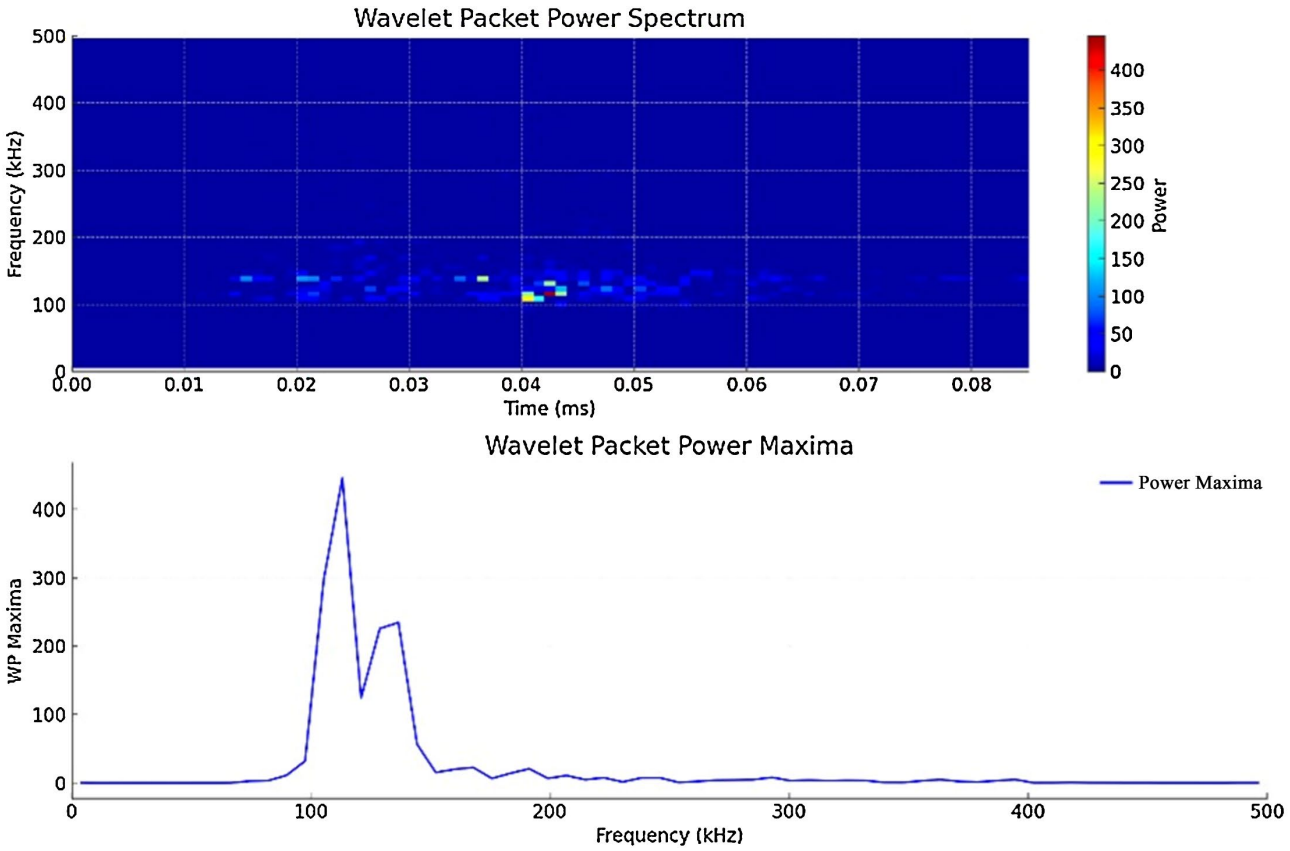

(c)

Figure 12. WPP spectrum and maxima of defect-induced AE signals.

rail defect signals emphasize the potential of using these AE characteristics for effective defect monitoring and diagnosis in rail systems.

7. Summary and Conclusions

The findings of this study demonstrate that AE signals generated by real-world rail defects exhibit distinct echo patterns at two distinct time scales, which are not observed in the PLB tests and which are less prevalent in the Nevada field tests. Preliminary assumptions suggest that these patterns may be induced by the superposition of internal reflections and multiple energy releases.

In contrast to the predictable attenuation characteristics observed in the PLB test, the attenuation behavior from the real-world field tests proved similar attenuation patterns. Environmental complexities in real-world scenarios, including increased mechanical vibrations and ambient noise likely interfere with AE propagation, resulting in reduced clarity of attenuation behavior. Despite this, rail defect-induced AE signals consistently exhibited significantly higher power concentrations, particularly in the lower frequency bands. Such sensitive power level in rail defect AE signals underscores the increased severity and intensity of acoustic emissions associated with structural flaws. This may serve as experimental evidence that presents the diagnostic potential of WPP analysis in detecting and eval-

uating defect severity.

The combined analyses demonstrate the ability of our approach to distinguish between AE signals from simulated sources (PLB) and actual rail defects based on their frequency content, attenuation behavior, and power distribution. The differences observed from our test scenarios suggest that AE monitoring systems can be more effective when tuned to specific frequency bands and attenuation behaviors associated with defect-related emissions. The findings also emphasize the importance of high-frequency range analysis, facilitated by high-pass filtering, to capture critical AE details that are indicative of defect presence and severity.

The research highlights the promising potential of air-coupled optical microphones for capturing AE signals without having direct contact with the rail. This non-contact approach can facilitate early-stage rail defect monitoring, enabling continuous inspection without disrupting regular train operations. The research results indicate that 2-inch is a critical point of reduction of AE signals, which provides guidance on setting up sensors in the field.

AE signal characteristics were investigated through a combination of controlled lab tests and real-world field tests. The results confirmed the capability of the developed method to detect internal defects, while limitations remain due to environmental noise and signal attenuation in operational settings. Preliminary evaluations of AE signals using CWT and WPP analysis revealed that AE signal propagation characteristics are highly dependent on test conditions. These analytical tools proved effective in differentiating between AE sources and in identifying signatures associated with defect severity. It should be noted that the noise floor was not measured in the test, which would add uncertainty in the results obtained in this study.

Overall, this research contributes meaningful insights to the safety assessment of rail infrastructure, ultimately enhancing rail maintenance and management. By advancing non-contact AE technology for real-time rail health monitoring, the study lays the groundwork for future developments in automated, scalable AE monitoring systems for railway infrastructure.

Acknowledgements and Declarations

This research is supported by the USDOT Tier 1 University Transportation Center on Improving Rail Transportation Infrastructure Sustainability and Durability under contract 69A3551747132. The authors declare that the contents of this article have not been published previously. All the authors have contributed to the work described, read and approved the contents for publication in this journal. All the authors have no conflict of interest with the funding entity and any organization mentioned in this article in the past three years that may have influenced the conduct of this research and the findings.

Conflicts of Interest

The authors declare no conflicts of interest regarding the publication of this paper.

References

[1] Rizzo, P. and Coccia, S. (2009) Noncontact Rail Monitoring by Ultrasonic Guided Waves. *Encyclopedia of Structural Health Monitoring*, **2397**, 2397-2410. https://doi.org/10.1002/9780470061626.shm041

[2] Li, D. (2018) Rail Crack Monitoring Using Acoustic Emission Technique. Springer. https://doi.org/10.1007/978-981-10-8348-8

[3] Fischer, B. (2016) Optical Microphone Hears Ultrasound. *Nature Photonics*, **10**, 356-358. https://doi.org/10.1038/nphoton.2016.95

[4] Lanza di Scalea, F., Rizzo, P., Coccia, S., Bartoli, I., Fateh, M., Viola, E., *et al.* (2005) Non-Contact Ultrasonic Inspection of Rails and Signal Processing for Automatic Defect Detection and Classification. *Insight—Non-Destructive Testing and Condition Monitoring*, **47**, 346-353. https://doi.org/10.1784/insi.47.6.346.66449

[5] Mariani, S., Nguyen, T., Zhu, X. and Lanza di Scalea, F. (2017) Field Test Performance of Noncontact Ultrasonic Rail Inspection System. *Journal of Transportation Engineering*, *Part A*: *Systems*, **143**. https://doi.org/10.1061/jtepbs.0000026

[6] Kim, N., Sohn, H. and Han, S. (2012) Rail Inspection Using Noncontact Laser Ultrasonics. *Journal of the Korean Society for Nondestructive Testing*, **32**, 696-702. https://doi.org/10.7779/jksnt.2012.32.6.696

[7] Lanza di Scalea, F., Zhu, X., Capriotti, M., Liang, A.Y., Mariani, S. and Sternini, S. (2017) Passive Extraction of Dynamic Transfer Function from Arbitrary Ambient Excitations: Application to High-Speed Rail Inspection from Wheel-Generated Waves. *Journal of Nondestructive Evaluation*, *Diagnostics and Prognostics of Engineering Systems*, **1**, Article ID: 011005. https://doi.org/10.1115/1.4037517

[8] Bruzelius, K. and Mba, D. (2004) An Initial Investigation on the Potential Applicability of Acoustic Emission to Rail Track Fault Detection. *NDT & E International*, **37**, 507-516. https://doi.org/10.1016/j.ndteint.2004.02.001

[9] Nivesrangsan, P., Steel, J.A. and Reuben, R.L. (2007) Source Location of Acoustic Emission in Diesel Engines. *Mechanical Systems and Signal Processing*, **21**, 1103-1114. https://doi.org/10.1016/j.ymssp.2005.12.010

[10] Zhang, X., Feng, N., Wang, Y. and Shen, Y. (2015) Acoustic Emission Detection of Rail Defect Based on Wavelet Transform and Shannon Entropy. *Journal of Sound and Vibration*, **339**, 419-432. https://doi.org/10.1016/j.jsv.2014.11.021

[11] Li, D., Wang, Y., Yan, W. and Ren, W. (2020) Acoustic Emission Wave Classification for Rail Crack Monitoring Based on Synchrosqueezed Wavelet Transform and Multi-Branch Convolutional Neural Network. *Structural Health Monitoring*, **20**, 1563-1582. https://doi.org/10.1177/1475921720922797